Causing the Effect: Driving the Unruh Response

Kevin Player*†

August 23, 2025

> The Unruh effect tells us that what we call particles is really just a matter of perspective.
>
> Lee Smolin

Abstract

We present a framework that connects the thermal Unruh effect to a localized, non-thermal excitation picture. Using modular automorphisms, we track mode localization across nested Rindler wedges and construct compact wave-packet approximations via parabolic cylinder functions. This yields a smooth transition from global Rindler modes to fully localized excitations, supporting a view that connects vacuum correlations with localized, directed excitations.

1 Introduction

The Unruh effect[1] shows how uniformly accelerated observers perceive the Minkowski vacuum as a thermal bath of particles. In this work, we develop a complementary viewpoint by examining, within our model, how localization can affect the thermal character of the field. In Section 2, we review the Unruh effect, including the relevant mode expansions and Bogoliubov transformations. In Section 3, we apply a bilocal version of a classical source construction to inject particles into the field.

Section 4 explores partial localization by considering sub-regions of the Rindler wedge related through space-like translations and reflections, transformations that correspond to modular automorphisms in the associated operator algebras. We then use parabolic cylinder functions to construct a smooth interpolation between eternal Rindler modes and fully localized modes. Finally, in Sections 5 and 6, we recommend future research and interpret the implications of our construction.

These results suggest that the Unruh effect can partially arise from localized, non-thermal excitations.

2 Preliminaries

We draw notation and standard results from Frodden and Valdés [2]. Let $\hbar = c = 1$. We follow the standard practice of working in 1+1 dimensional Minkowski spacetime with free, massless scalar fields, which isolates the essential features of the Unruh effect

*kplayer@andrew.cmu.edu
†kjplaye@gmail.com

without the technical overhead of higher dimensions or interactions. These simplifications do not alter the key physics, but make the structure of mode localization transparent.

Consider the free scalar massless Lagrangian

$$\mathcal{L}_{free} = -\frac{1}{2}\eta^{\mu\nu}\partial_\mu\phi\partial_\nu\phi. \tag{1}$$

We consider positive frequency modes with dispersion relation $\omega_k = |k| > 0$ as solutions to the resulting Klein-Gordon equation

$$\Box\phi = -\frac{\partial^2\phi}{\partial t^2} + \frac{\partial^2\phi}{\partial x^2} = 0, \tag{2}$$

where $\Box = \eta^{\mu\nu}\partial_\mu\partial_\nu$. We expand ϕ in terms of ladder operators $a_k, a_k^\dagger$

$$\phi(x,t) = \int \mathrm{d}k\, a_k\varphi_k(x,t) + \text{h.c.} \tag{3}$$

where

$$\varphi_k(x,t) = \frac{1}{\sqrt{4\pi\omega_k}}e^{i(kx-\omega_k t)}. \tag{4}$$

are pure Minkowkski positive frequency waves normalized with respect to the Klein-Gordon inner product over a Cauchy surface Σ (usually $t = 0$)

$$\langle f, g\rangle_{KG} = i\int_\Sigma \mathrm{d}x(f^*\partial_t g - \partial_t f^* g). \tag{5}$$

2.1 Rindler Coordinates

To describe the physics from the point of view of a uniformly accelerating observer, we introduce Rindler coordinates [2, 3] covering a right wedge

$$W = \{(x,t) : x > |t|\} \tag{6}$$

with apex at the origin, pictured[1] in Figure 1; with coordinates

$$t = \frac{1}{a}e^{a\xi}\sinh(a\eta) \tag{7}$$

$$x = \frac{1}{a}e^{a\xi}\cosh(a\eta) \tag{8}$$

The constant acceleration parameter a is introduced explicitly to make the dependence on the Unruh temperature, $T = \frac{a}{2\pi}$, manifest in subsequent expressions. The coordinates (η, ξ) describe the proper time and position in the frame of a uniformly accelerating observer, with world-lines of constant ξ corresponding to hyperbolic trajectories in Minkowski space-time.

The massless Klein-Gordon equation in Rindler coordinates is

$$\Box\phi = e^{-2a\xi}(-\partial_\eta^2 + \partial_\xi^2)\phi = 0 \tag{9}$$

The wave equation retains the same structure as the Minkowski case, up to the overall conformal factor $e^{-2a\xi}$. Since this factor does not affect the null structure of the equation, the mode solutions retain the same plane wave form but in the Rindler coordinates

$$r_k(\eta,\xi) = \frac{1}{\sqrt{4\pi\omega_k}}e^{-i(\omega_k\eta - k\xi)} + \text{h.c.} \tag{10}$$

for each wave number k and positive frequency $\omega_k = |k| > 0$. These "Rindler modes" are in terms of η and ξ and are thus confined to the Rindler wedge W. Since Rindler coordinates only cover W (the right wedge), these modes are not defined globally in Minkowski space.

[1] All diagrams follow the convention of t increasing upward and x increasing to the right.

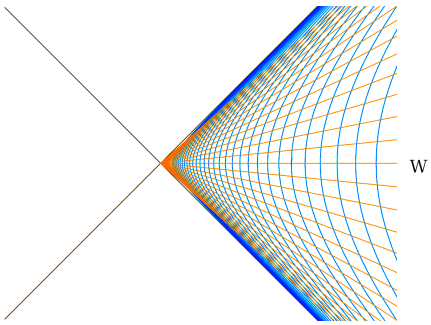

Figure 1: Rindler wedge W on the right.

2.2 Unruh Modes

To review how a uniformly accelerated observer perceives the Minkowski vacuum as a thermal bath, we construct the Unruh modes[1], analytic continuations of Rindler modes that are positive-frequency solutions with respect to Minkowski time[2]. From now on let $\omega_k = k > 0$.

We define constants α_k and β_k, directly tied the the thermal description, which satisfy $\alpha_k^2 - \beta_k^2 = 1$

$$\begin{aligned} \alpha_k &= \frac{e^{\frac{\pi\omega_k}{2a}}}{\sqrt{2\sinh\frac{\pi\omega_k}{a}}} = \sqrt{\frac{1}{1-e^{-2\pi\omega_k/a}}} = \sinh\theta_k \\ \beta_k &= \frac{e^{\frac{-\pi\omega_k}{2a}}}{\sqrt{2\sinh\frac{\pi\omega_k}{a}}} = \sqrt{\frac{1}{e^{2\pi\omega_k/a}-1}} = \cosh\theta_k \quad \text{(thermal form)} \end{aligned} \tag{11}$$

where θ_k is defined so that $\tanh\theta_k = \frac{\beta_k}{\alpha_k} = e^{-\pi\omega_k/a}$. These show up throughout in mode normalizations[3], inner products, and resulting Bogoliubov transforms. β_k also describes particle creation in terms of $|\beta_k|^2$ which has a thermal character, matching a Planck distribution at temperature $T = \frac{a}{2\pi}$.

Let $\widetilde{W}$ be the left Rindler wedge[4], $x < -|t|$ with Rindler modes $l_{\pm k}$. We analytically continue[5] the Rindler modes r_k, r_{-k}, l_k and l_{-k} into the (t,x) plane, these are the Unruh modes

$$\begin{aligned} \mu^R_{\pm k} &= \tfrac{\alpha_k}{\sqrt{4\pi\omega_k}}(a(\mp t + x \pm i\epsilon))^{\pm\frac{i\omega_k}{a}} & \mu^R_{\pm k|_W} &\to \alpha_k r_{\pm k} \\ \mu^L_{\pm k} &= \tfrac{\alpha_k}{\sqrt{4\pi\omega_k}}(a(\mp t - x \pm i\epsilon))^{\pm\frac{i\omega_k}{a}} & \mu^L_{\pm k|_{\widetilde{W}}} &\to \alpha_k l_{\pm k} \end{aligned} \tag{12}$$

We added an $i\epsilon$ prescription to dictate which branch of the log to take so that the modes are analytic and bounded on the $\Im(t) < 0$ half plane. This makes the modes positive-frequency with respect to t. Another way of writing the Unruh modes is

$$\begin{aligned} \mu^R_{\pm k} &= \alpha_k r_{\pm k} + \beta_k l^*_{\mp k} \\ \mu^L_{\pm k} &= \alpha_k l_{\pm k} + \beta_k r^*_{\mp k} \end{aligned} \tag{13}$$

where the right and left modes ($r_{\pm k}$ and $l_{\pm k}$) are understood to be zero outside of their respective wedges. See Figure 2 for an illustration of the various modes. The magnitude shown jumps across the branch cut and conjugates the phase. Also, note that we have

[2]The modes contain no negative frequency Minkowski components.

[3]The normalizations come from computing the Klein Gordon inner product on Minkowski space and comparing it to inner products on W and $\widetilde{W}$.

[4]Coordinates on this wedge are $t = -\frac{1}{a}e^{a\delta}\sinh(a\gamma)$, $x = -\frac{1}{a}e^{a\delta}\cosh(a\gamma)$; and $l_{\pm k} = \frac{1}{\sqrt{4\pi\omega_k}}e^{i\omega_k(\gamma\pm\delta)}$.

[5]From the definitions and properties of sinh and cosh, it follows that $a(\pm t + x) = e^{a(\pm\eta+\xi)}$ and then $r_{\pm k} = e^{\pm\frac{i\omega_k}{a}\log a(\mp t+x\pm i\epsilon)}$. Similar statements hold for the left wedge.

"twice as many" Unruh modes as we have Rindler modes; we double count each r_k with two analytic extensions μ_k^R and μ_{-k}^{L*}, and similarly for the left modes.

The Unruh modes form an alternative orthonormal basis of solutions to the Klein-Gordon equation, distinct from the plane waves $\varphi_{\pm k}$ see the original source Unruh[1]. The Unruh modes diagonalize (we will see in equation (17)) the Minkowski vacuum in terms of Rindler particle states and thus provide the natural framework for describing the Unruh effect and the thermal response perceived by uniformly accelerated observers.

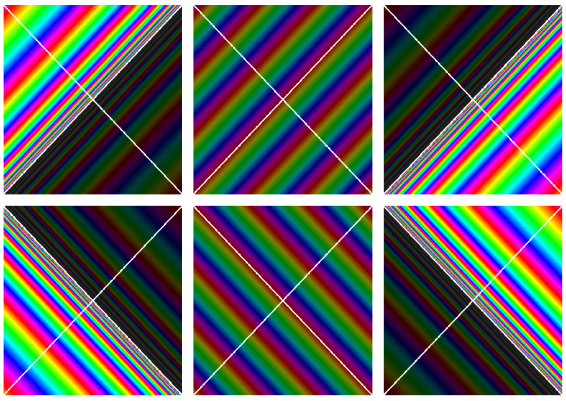

Figure 2: Spacetime diagrams of the $k > 0$ mode functions $\begin{bmatrix} \mu_{-k}^L & \varphi_k & \mu_k^R \\ \mu_k^L & \varphi_{-k} & \mu_{-k}^R \end{bmatrix}$ where μ and φ are Unruh modes and Minkowski mode respectively. Color encodes the phase; brightness indicates magnitude. The Unruh modes change magnitude and conjugate phase across the log branch due to the interpretation of $\log(-1 \pm i\epsilon)$. The left-moving modes (top) correspond to emission in Minkowski space; the right-moving modes (bottom) to absorption.

2.3 Bogoliubov Transforms

We generalize the wedge W to a translated wedge W_c with apex $(0, c)$

$$W_c = \{(t, x) : x - c > |t|\} \tag{14}$$

and a reflected (left) wedge $\widetilde{W}_c$ with apex $(0, c)$

$$\widetilde{W}_c = \{(t, x) : x - c < -|t|\}. \tag{15}$$

Let the superscripts (0), (c), $(\widetilde{c})$, and (M) represent the W_0, W_c, $\widetilde{W}_c$, and Minkowski frames of reference respectively. Let $(A \to B)$ represent an open set inclusion[6] $A \subseteq B$.

This allows us to directly compute $W_0 \to M$ Bogoliubov coefficients from equation (13) for a change of basis from $a_q^{(M)}$ to c_q^R and c_q^L

$$\phi = \int \mathrm{d}q \; \mu_q^R c_q^R + \mu_q^L c_q^L + \text{h.c.} \tag{16}$$

We find a 4 by 4 block matrix with blocks of the form

$$\begin{bmatrix} a_k^{(0)} \\ \\ a_{-k}^{\widetilde{(0)}\dagger} \end{bmatrix} = \begin{bmatrix} \alpha_k & \beta_k \\ \beta_k & \alpha_k \end{bmatrix} \begin{bmatrix} c_k^R \\ c_{-k}^{L\dagger} \end{bmatrix} \tag{17}$$

[6]In the algebraic formulation of QFT, spacetime regions correspond to operator algebras. Here, we adopt a complementary (though formally contravariant) perspective, whereby shifts in the wedge induce Bogoliubov transformations between operator algebras.

and three others, where the $a_{-k}^{\widetilde{(0)}\dagger}$ is a left wedge creation operator. We can summarize the transform in the right wedge W as

$$a_k^{(0)} = \alpha_k c_k^R + \beta_k c_{-k}^{L\dagger} \tag{18}$$

and three other similar relations for $a_{-k}^{(0)}$, $a_k^{(0)\dagger}$, and $a_{-k}^{(0)\dagger}$.

We next compute the more general non-diagonal mixed Bogoliubov transformations.

$$\begin{array}{rrl} (c \to M): & a_k^{(c)} & = \int \mathrm{d}q\ \alpha_{kq}^{(c\to M)} a_q^M + \beta_{kq}^{(c\to M)} a_q^{(M)\dagger} \\ (c \to 0): & a_k^{(c)} & = \int \mathrm{d}q\ \alpha_{kq}^{(c\to 0)} a_q^{(0)} + \beta_{kq}^{(c\to 0)} a_q^{(0)\dagger} \\ (\widetilde{c} \to 0): & a_k^{(\widetilde{c})} & = \int \mathrm{d}q\ \alpha_{kq}^{(\widetilde{c}\to 0)} a_q^{(0)} + \beta_{kq}^{(\widetilde{c}\to 0)} a_q^{(0)\dagger} \end{array} \tag{19}$$

We make use of a gamma function for $(c \to M)$. This occurs naturally in the KG dot product as an integral over an exponential phase from φ_k and a $(x-c)$ power from $r_k^{(c)}$ (the Mellin transform of e^{ikx} [4]):

$$\begin{array}{lll} \alpha_{kq}^{(c\to M)} & = \left\langle \varphi_q, r_k^{(c)} \right\rangle & = \frac{1}{2\pi a}\sqrt{\frac{\omega_k}{\omega_q}} \left(\frac{a}{q}\right)^{\frac{i\omega_k}{a}} e^{\frac{\pi\omega_k}{2a}} \Gamma\left(\frac{i\omega_k}{a}\right) \\ \beta_{kq}^{(c\to M)} & = \left\langle \varphi_q^*, r_k^{(c)} \right\rangle & = \frac{1}{2\pi a}\sqrt{\frac{\omega_k}{\omega_q}} \left(\frac{a}{q}\right)^{\frac{i\omega_k}{a}} e^{\frac{-\pi\omega_k}{2a}} \Gamma\left(\frac{i\omega_k}{a}\right) \end{array} \tag{20}$$

Next we consider products of shifted powers to go after $(c \to 0)$. We make use of a beta function for $(c \to 0)$ which occurs naturally in the KG dot product as an integral over a power of x and of $x-c$, from $r_k^{(0)}$ and $r_k^{(c)}$ respectively. We compute the Bogoliubov coefficients as

$$\begin{aligned} \alpha_{kq}^{(c\to 0)} &= \left\langle r_q^{(0)}, r_k^{(c)} \right\rangle = \frac{1}{2\pi a}\sqrt{\frac{\omega_k}{\omega_q}} (ac)^{\frac{i(\omega_k-\omega_q)}{a}} B\left(\frac{i\omega_k}{a}, \frac{-i(\omega_k-\omega_q)}{a}\right) \\ \beta_{kq}^{(c\to 0)} &= \left\langle r_q^{(0)*}, r_k^{(c)} \right\rangle = \frac{1}{2\pi a}\sqrt{\frac{\omega_k}{\omega_q}} (ac)^{\frac{i(\omega_k+\omega_q)}{a}} B\left(\frac{i\omega_k}{a}, \frac{-i(\omega_k+\omega_q)}{a}\right) \end{aligned} \tag{21}$$

The reflected diamond wedge version also yields a beta function, but with a different form

$$\begin{aligned} \alpha_{kq}^{(\widetilde{c}\to 0)} &= \left\langle r_q^{(0)*}, r_k^{(\widetilde{c})} \right\rangle = \frac{1}{2\pi a}\frac{\sqrt{\omega_k\omega_q}}{\omega_q-\omega_k} (ac)^{\frac{i(\omega_k-\omega_q)}{a}} B\left(\frac{i\omega_k}{a}, -\frac{i\omega_q}{a}\right) \\ \beta_{kq}^{(\widetilde{c}\to 0)} &= \left\langle r_q^{(0)}, r_k^{(\widetilde{c})} \right\rangle = \frac{1}{2\pi a}\frac{\sqrt{\omega_k\omega_q}}{\omega_q+\omega_k} (ac)^{\frac{i(\omega_k+\omega_q)}{a}} B\left(\frac{i\omega_k}{a}, \frac{i\omega_q}{a}\right) \end{aligned} \tag{22}$$

2.4 Modular Automorphisms

We can compare absolute magnitudes for M v.s. W_c and see that they don't depend on c

$$\begin{aligned} \left|\alpha_{sq}^{(c_1\to M)}\right|^2 &= \left|\alpha_{kq}^{(c_2\to M)}\right|^2 \\ \left|\beta_{kq}^{(c_1\to M)}\right|^2 &= \left|\beta_{kq}^{(c_2\to M)}\right|^2 \end{aligned} \tag{23}$$

The c independence is expected in this case since Unruh radiation is translation invariant. We next turn to $(c \to 0)$ and also find c independence there

$$\begin{aligned} \left|\alpha_{kq}^{(c_1\to 0)}\right| &= \left|\alpha_{kq}^{(c_2\to 0)}\right| \\ \left|\beta_{kq}^{(c_1\to 0)}\right| &= \left|\beta_{kq}^{(c_2\to 0)}\right| \end{aligned} \tag{24}$$

This invariance is more surprising than in the Minkowski case, as it implies that the expected number of excitations for a mode $r_k^{(c_2)}$ when expressed in the vacuum of W_{c_1},

$$\int \mathrm{d}q\ |\beta_{kq}^{(c_2\to c_1)}|^2 \tag{25}$$

is invariant[7] under changes in both c_1 and c_2.

More explicitly using the form of the c term in equations (21) and (22) we have a transform matrix of Λ_c from W_0 to W_c

$$\begin{bmatrix} a_k^{(c)} \\ a_{-k}^{(c)} \\ \hline a_k^{(c)\dagger} \\ a_{-k}^{(c)\dagger} \end{bmatrix} = \underbrace{\left[\begin{array}{cc|cc} A_c & 0 & B_c & 0 \\ 0 & -A_c & 0 & -B_c \\ \hline \overline{B_c} & 0 & \overline{A_c} & 0 \\ 0 & -\overline{B_c} & 0 & -\overline{A_c} \end{array}\right]_{k,q}}_{\Lambda_c} \begin{bmatrix} a_q^{(0)} \\ a_{-q}^{(0)} \\ \hline a_q^{(0)\dagger} \\ a_{-q}^{(0)\dagger} \end{bmatrix} \tag{26}$$

where $A_c = \alpha_{kq}^{(c\to 0)} = P_c A_1 P_c^{-1}$ and $B_c = \beta_{kq}^{(c\to 0)} = P_c B_1 P_c$ for a diagonal phase factor matrix

$$P_{c,rs} = \delta(r-s)c^{\frac{i\omega_r}{a}} = e^{\frac{iH}{a}\log c} \tag{27}$$

where H is the Rindler Hamiltonian associated with mode frequency ω_k. We can write Λ_c out compactly out as

$$\Lambda_c = Q_c \Lambda_1 Q_c^{-1} \tag{28}$$

where

$$Q_c = \begin{bmatrix} P_c, & 0 & 0 & 0 \\ 0 & P_c & 0 & 0 \\ 0 & 0 & P_c^{-1} & 0 \\ 0 & 0 & 0 & P_c^{-1} \end{bmatrix} \tag{29}$$

The composition of Bogoliubov transforms, $\Lambda_{nc} = \Lambda_c^n$, yields

$$\begin{aligned} Q_{nc}\Lambda_1 Q_{nc}^{-1} &= \Lambda_{nc} \\ &= (Q_c \Lambda_c Q_c)\left(Q_c^{-1}\Lambda_c Q_c\right)\cdots(Q_c\Lambda_c Q_c) \\ &= Q_c \Lambda_c^n Q_c^{-1} \end{aligned} \tag{30}$$

so that

$$\begin{aligned} \Lambda_c^n &= Q_c^{-1} Q_{nc}\Lambda_1 Q_{nc}^{-1} Qc \\ &= Q_n \Lambda_1 Q_n^{-1} \end{aligned} \tag{31}$$

and more generally we have a one parameter unitary group under the modular parameter $x = \log c$, with generator H/a given by

$$\left\{\Lambda_1^x = Q_x \Lambda_1 Q_x^{-1} : x \in \mathbb{R}\right\}. \tag{32}$$

So these Bogoliubov transformations between shifted wedges form a one-parameter group under translations of the apex, exhibiting a symmetry that parallels modular automorphism flow in algebraic QFT [5]. In contrast to traditional treatments emphasizing Lorentz boosts within a fixed wedge, this formulation reveals modular structure via spatial translations.

Consider a sequence

$$W_{c_n} \subseteq \cdots \subseteq W_{c_i} \subseteq \cdots \subseteq W_{c_j} \subseteq W_{c_2} \subseteq W_{c_1} \tag{33}$$

The result is that each inclusion $W_{c_i} \subseteq W_{c_j}$ yields the same "amount" and "type" of particle production, with fixed squared Bogoliubov magnitude $|\beta_{kq}|^2$, implying that the expected number of particles remains constant across all nested wedge pairs, independent of the actual values of c_i or c_j. We will briefly revisit this chain in Section 3.4.

[7]Similar statements are true for reflected (diamond) wedges.

3 Driving Sources

We now turn to a foundational question: **What, physically, is accelerating the observer?"** In standard Unruh-effect derivations, the acceleration is treated as given; here we supply a concrete mechanism in the form of a localized, entangled source, thereby shifting from kinematic bookkeeping to a dynamical, source-based picture.

In Section 2 we introduced acceleration as a geometric feature, a coordinate choice, without reference to any underlying dynamical mechanism. Moreover, we have left unspecified both the observer's precise location within the Rindler wedge and the spatial origin of the detected excitations. These omissions reflect an effective coarse-graining over the details of the observer and their interaction with the field, a feature that contributes to the apparent thermality observed in the Unruh effect.

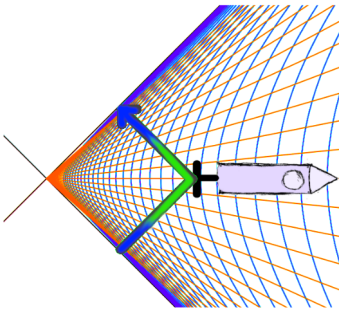

Figure 3: A Rindler mode's frequency is smeared out in Minkowski space, blue-shifted near the horizon, and red-shifted as x goes to positive infinity. We diagram a particle as if it were striking a moving mirror at the rear of a rocket, where its reflection emerges as a combination of emission and absorption processes in the Rindler frame.

A natural physical interpretation is that a *driving source* must exist, both as the cause of the observer's acceleration, and as a localized source coupled to the quantum field. In this view, acceleration is not merely a kinematic artifact or coordinate reparameterization, but the result of active, localized interactions along the observer's worldline. These interactions are responsible for the observer's motion. This plays well with the notion that the observer is not in an isotropic background radiation, but is actually thrusted away from a thermal event horizon, the thrust being intimately correlated with the causal horizon.

Figure 3 illustrates the situation with a particle composed of Rindler modes on the right wedge. The modes r_k are left-moving, propagating toward the future horizon and associated with **emission**; the r_{-k} modes are right-moving, originating from the past horizon and are associated with **absorption**. These Rindler modes are constructed as superpositions of restricted Minkowski modes $\varphi_{q|_W}$ effectively smeared across a range of frequencies. This frequency mixing is evident in Figure 2, where the modes blue-shift infinitely near the horizons and red-shift infinitely at spatial infinity, reflecting the geometry of the wedge.

3.1 Construction

We begin our construction of a driving source using an Alice and Bob style example pictured in Figure 4, using the names Wright(R), Lester(L), and Paz(P) to represent Right, Left, and Past observers at locations (t,x) = (0,1), (0,-1) and (-1,0) respectively. Paz serves as a common causal ancestor to Wright and Lester. Paz emits an entangled pair of photons with momentum $\pm k$ and (Rindler) frequency $\omega = \omega_{\pm k}$ as part of a stream

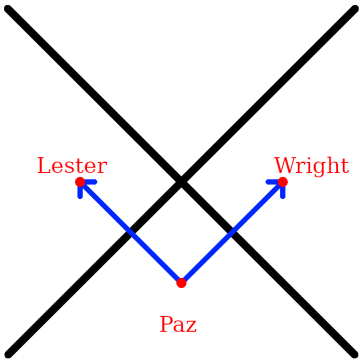

Figure 4: A thruster in the past, Paz(P), emits an entangled photon pair that accelerates Wright(R) (to the right) and Lester(L) (to the left).

of photons that are in our model the source, and cause, of the acceleration of Wright and of Lester. The accelerations are thus correlated.

Because the emitted photons carry perfectly balanced momenta, our basic model exhibits no back reaction. This simplification is purely kinematic; in more general models, single-particle sources would encode back reaction through their entanglement structure (see Section 3.2 and Figure 7)."

Now where we usually would create a localized detector for Wright, such as an Unruh-DeWitt detector [1] [6] or a moving mirror[8] [7] interacting with the field, we instead seek to model the situation where Paz, a *thruster*, is coupled to the field in the past. This inversion of effect and cause, of detector and thruster, is at the heart of our construction; we deliberately invert the usual order, instead of positing acceleration and deriving entanglement, we posit an entangled source and derive acceleration.

Paz's emission makes the source of the acceleration manifest as particle injection, so that Wright will make sense of a *guaranteed* observation of a "thrust particle" with fixed peaked right moving momentum $-k$. Wright's detection is entangled with Lester's, so Lester will also observe a particle with left moving momentum k; measurement induced correlation.

Physically, Paz introduces a bilocal source

$$\begin{aligned} J(x,y) &= \lambda f_L(x) f_R(y) \\ \mathcal{L}_{sourced} &= \mathcal{L}_{free} + \frac{1}{2}\lambda \int f_L(x) f_R(y) \phi_+(x) \phi_+(y) + h.c. \\ &= \mathcal{L}_{free} + \frac{1}{2}\lambda \left(q_k^{L\dagger} q_{-k}^{R\dagger} + q_k^L q_{-k}^R \right) \end{aligned} \tag{34}$$

with coupling constant λ, normalized mode profiles f_L and f_R supported on the left and right wedges respectively, creation operators $q_k^{L\dagger}$ and $q_{-k}^{R\dagger}$, and ϕ_+ as the positive frequency (annihilator) part of ϕ. The last part of equation (34) is the squeezing interaction for frequency ω, so that the bilocal source creates particles in the Rindler basis within the wedges.

We consider the case where f_L and f_R are absorptions, or made up of left moving and right moving Minkowkski modes respectively; the emission case is similar see Section 3.3. In this picture, the bilocal source is not just a mathematical device but the physical mechanism by which acceleration is generated: the entangled pair created by $J(x,y)$ supplies the correlated excitations that are experienced as thrust by the Rindler observers.

[8]While a moving mirror can be interpreted as a type of thruster that reshapes the field through boundary acceleration, here we isolate the thruster from the detector role. Incorporating the moving mirror timeline localizations into our model is left for future research.

This source construction is a straightforward quadratic generalization of the usual linear source term [8] [9] and is motivated by quadrature squeezed light generation in quantum optics [10]; it is a coupling of a classical function J with the field as an interaction term smeared over x and y. In this version J squeezes the field creating correlations that manifest as entanglement at the level of a global quantum state. The product structure reflects this paired excitation.

Smearing with ϕ_+ projects f_L and f_R onto their positive frequency parts which we call g_L and g_R respectively. In particular we can choose f_L and f_R to be Rindler modes l_k and r_{-k} in which case the projection is onto the corresponding Unruh modes μ_k and μ_{-k}, so that $q_k^{L\dagger}$ and $q_{-k}^{R\dagger}$ are the corresponding Unruh operators $c_k^{L\dagger}$ and $c_{-k}^{R\dagger}$ from equation (16).

Table 1: Bilocal Source – Modes, Operators, and States

Type	Source	Projection	Operator	State (1st order)
General Left	f_L	g_L	$q_k^{L\dagger}$	$\|\psi\rangle_L$
General Right	f_R	g_R	$q_{-k}^{R\dagger}$	$\|\psi\rangle_R$
Unruh/Rindler Left	l_k	μ_k^L	$c_k^{L\dagger}$	$\|1_\omega\rangle_L$
Unruh/Rindler Right	r_{-k}	μ_{-k}^R	$c_{-k}^{R\dagger}$	$\|1_\omega\rangle_R$

We next consider the standard thermal vacuum description[9] of the Unruh effect

$$|0\rangle_M = \prod_\omega \frac{1}{\cosh\theta_k} \sum_n \tanh^n\theta_k \, |n_\omega\rangle_L \, |n_\omega\rangle_R \, . \tag{35}$$

A state that factorizes into correlated excitations in the left (L) and right (R) wedges. The Unruh modes associated with frequency ω are specific linear combination of these L and R Rindler modes, so that any source J coupling to it will, in general, drive correlated excitations across both wedges. For example, the state prepared by Paz with Rindler modes corresponds to a selective excitation at a fixed ω,

$$|\Psi_\omega\rangle = |1_\omega\rangle_L \, |1_\omega\rangle_R + \mathrm{O}(\text{higher terms}), \tag{36}$$

a controlled realization of one term in the ensemble coming from the Rindler/Unruh modes. Our source projects the state onto the ω term through the act of observation, i.e. by a PVM projection in the standard quantum-measurement sense, so that Wright's guaranteed detection is modeled as the measurement-induced selection of a specific component of the thermal ensemble. The source $J(x, y)$ does not contradict the thermal interpretation, but rather describes a specific "microstate" consistent with the broader thermal ensemble.

An illustration of this setup is shown in Figure 5. From this perspective, the apparent thermality arises from intrinsic properties of the vacuum, an effective ignorance of the source's detailed structure and dynamics. In the sourced view, the Unruh effect is not a passive revelation of hidden particles in the vacuum, but a measurable consequence of *thrust*.

3.2 Physical Details

The construction of a right moving absorption function f_R for Wright presents some physical challenges. The first starts with a note that the f_L and f_R that match equation (36) are exactly the Rindler modes l_k and r_{-k} from Section 2. The J is described in the Rindler wedges, and not immediately on the past wedge, so Paz will need to couple to

[9]The form of this vacuum equation can be proven by recursively applying the Bogoliubov relations in equation (18).

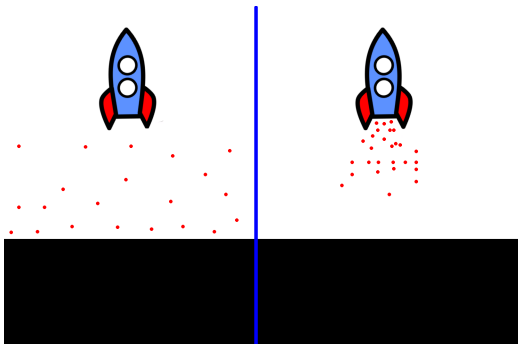

Figure 5: Conceptual illustration of thermal v.s. localized acceleration.

Unruh modes – the analytically continued Rindler modes. We form f_R out of a linear combination of a left Unruh mode μ_k^{L*} and right Unruh mode μ_{-k}^R to get r_{-k} supported on just the right wedge, see equation (13). The projection in equation (34) encodes this relation by projecting the Rindler modes onto Unruh modes or in more generality by projecting f_L and f_R onto positive frequency g_L and g_R.

Another challenge is that we are integrating over the entire Minkowski space instead of over a short time period as normally desired for a source J. This challenge is met by noticing that the projected positive frequency modes g_L and g_R can be restricted and scaled on a small time interval $|t+1| < \delta$ around Paz's time $t = -1$ to give the same result, see Figure 6 (right picture). This is because we can write the integral as a foliation over equal time Cauchy surfaces, which each have the same integral by Stokes' theorem. It is also manifestly evident by the fact that the mode is translation invariant over time and space, $g_R(t,x) = g_R(-1, x+t+1)$, since it is a sum of right moving Minkowski modes. The coupling constant λ in equation (34), along with δ, can be chosen to match the vacuum equation (35) at $n_\omega = 1$.

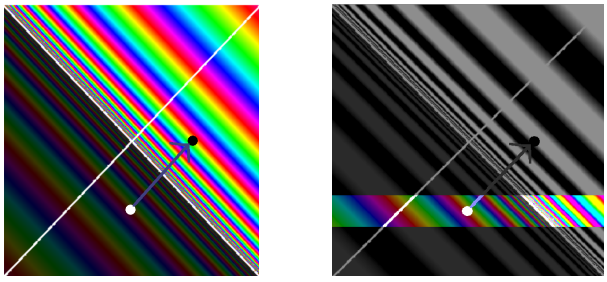

Figure 6: The points marked with black and white dots at (0,1) (Wright) and (-1,0) (Paz) respectively in the left picture lie on the same Unruh mode trajectory; although the mode is infinitely blue-shifted at the horizon, it settles down at Wright and Paz's locations. The right figure illustrates a finite time interval of width δ for the source J to be active.

A third note is that the Unruh modes undergo an infinite blue shift at the horizon, but are more well behaved at Wright and Paz's locations. f_R is actually zero at Paz and in fact on the entire past wedge, but the projection is to an Unruh mode which is nonzero at Paz. We study the localization of functions on the right wedge in subsequent sections where we aim to localize f_R away from the high-frequency, near-horizon behavior typical of thermal modes, making the physical realization of the source J more plausible as a localized wave packet.

Finally, we emphasize that our running example represents just one of many possible mechanisms for exchanging energy and correlations between wedges; for example, in our

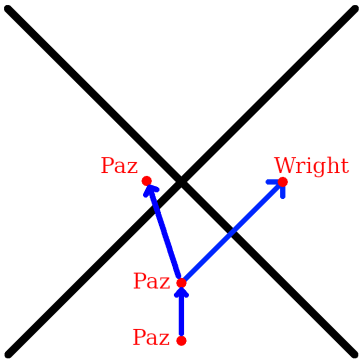

Figure 7: Paz emits a single photon and experiences a back reaction pushing her toward the left wedge. Through recoil she becomes entangled with the emitted particle, effectively taking on the role that Lester played in the symmetric construction.

symmetric two–mode setup, the momenta are balanced and the source does not experience recoil, so there is no back reaction at leading order. By contrast, if Paz emitted a single particle, as in Figure 7, the emitted mode would necessarily be entangled with Paz's internal state and/or recoil momentum, producing back reaction as field–source entanglement. Tracing out the source would leave Wright with a mixed state, and the apparent thermality would then arise from this entanglement with the thruster's degrees of freedom. Our choice of a balanced bilocal source thus isolates the thrust mechanism while postponing the additional complication of explicit source recoil for future research.

We also could study the emission case; where f_L and f_R are made up of right moving and left moving Minkowski modes respectively, see the next section for a time inversion story. These cases involve additional complications beyond the scope of our note and are a topic of future research.

For the remainder of this note, we focus on the function f_R in the right wedge without explicit reference to f_L, operating under the assumption that the localized driving source in the right wedge arises from a globally entangled paired source.

3.3 Back in Time Story

The following discussion should be read as a heuristic narrative rather than a literal dynamical account; it illustrates how the time orientation of Rindler wedges lends itself to a "back in time" story that mirrors the entanglement structure. Lester's proper time (Rindler time) in the left wedge is flowing in reverse to Minkowski time. So we can actually track the story as:

1. Lester emits a particle traveling back in time.
2. Paz receives this particle and reflects it forward in time to Wright.
3. Wright then absorbs the particle.

The presence of virtual particle-antiparticle pairs in massive scalar fields further enriches this picture, where antiparticles are understood as particles moving "back in time", though this extension lies beyond the scope of this present note.

We can interchange these emission and absorption stories, Wright emits and Lester absorbs, but we would need to involve an observer in the future at $(t, x) = (1, 0)$ for that.

3.4 Sub-Wedge Causal Chain

The sub-wedge sequence mentioned in equation (33) has an interesting interpretation. The vacuums are entangled from each wedge to the next sub-wedge. In our in construction, this is understood as a causal chain from Paz to Wright. Each sub-wedge inherits a source J from the previous.

4 Localization

Up to now, our modes have been perfectly sharp in Rindler frequency. We now construct localized packets to show the source picture survives realistic smearing. Also, from here on we often interchange "Rindler" and "Unruh" modes when referring to their restriction to a single wedge, since our focus is on the localized support rather than global analyticity.

4.1 Localization via Translated Wedge Inclusion

Consider the two nested Rindler wedges $W_c \subseteq W_0$ shown in Figure 8. Let r_q denote a Rindler mode[10] associated with W_0, analytically continued to the entire Minkowski space. The gray-scale region indicates the full support of r_q, while the rainbow-colored segment shows its restriction to the sub-wedge W_c.

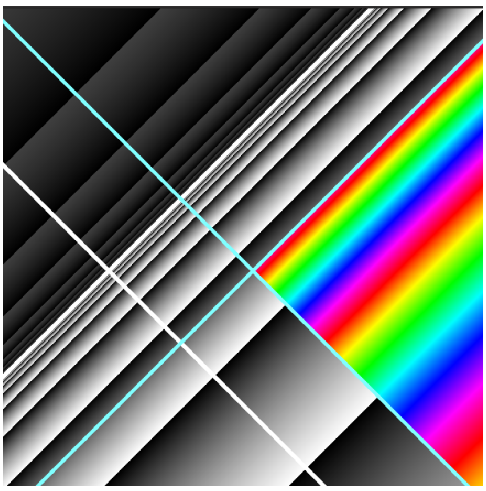

Figure 8: A Wedge W_c (cyan) inside of the wedge W_0 (white). Rindler mode r_q of W_0 (gray-scale) restricted to W_c (rainbow).

By considering the restriction of r_q to W_c, we have partially localized the observer and the mode. The restriction effectively cuts off the high-frequency content of r_q near the future horizon[11] of W_0. The resulting mode still spans the full spatial extent of W_c, but it is now insulated from the highly oscillatory behavior near the horizons of W_0. The localization is not complete however, the observer can still be anywhere within the wedge W_c, and the corresponding modes r_k still exhibit thermal characteristics because of low-frequency oscillations extending throughout the wedge.

To further study the situation, consider the modulus squared inner product $\left|\left\langle r_q^{(0)}, r_k^{(c)} \right\rangle\right|^2$, also known as the Bogoliubov $\left|\alpha_{kq}^{(c\to 0)}\right|^2$, from equation (21). We fix q and use $|\Gamma(ib)|^2 =$

[10] From here on we often interchange Rindler and Unruh modes since we are only concerned with the restriction to the right wedge or subsets.

[11] Similarly, r_{-q} experiences suppression near the past horizon.

$\frac{\pi}{b \sinh \pi b}$ to obtain

$$\left| \left\langle r_q^{(0)}, r_k^{(c)} \right\rangle \right|^2 = \frac{\sinh \frac{\pi \omega_q}{a}}{4\pi a(\omega_q - \omega_k) \sinh \pi \frac{\omega_q - \omega_k}{a} \sinh \frac{\pi \omega_k}{a}} \tag{37}$$

as a function of ω_k. The function exhibits a second-order pole at $\omega_k = \omega_q$, resulting in a sharply peaked feature, see Figure 9. Although the sinh terms encode aspects of the familiar thermal distribution, especially broadening near $\omega_k = 0$, the existence of the peak itself at $\omega_k = \omega_q$ originates from the geometric restriction, not from a detector's passive response to the vacuum, but as the active spectral footprint of a localized source.

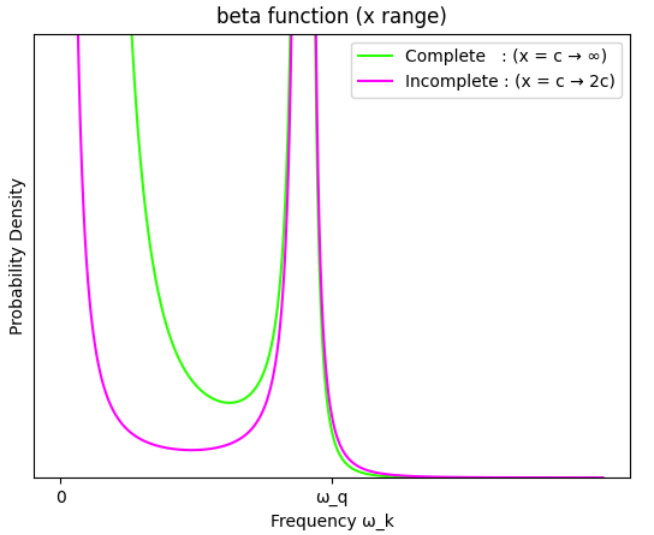

Figure 9: The Rindler modes r_k of W_c show a peaked spectral overlap with r_q at $\omega_k = \omega_q$. The incomplete beta function picks out the spectral peak suppressing the peak at zero.

4.2 Diamond Localization via Reflected Wedge Intersection

Further localization is achieved by intersecting W_c with a reflected wedge $\widetilde{W_{2c}}$. This defines a more tightly localized diamond-shaped region, as shown in Figure 10. The mode r_q is now restricted to the intersection $W_c \cap \widetilde{W_{2c}}$, which eliminates much of the infrared behavior previously associated with the unrestricted wedge.

The Klein Gordon inner product at $t = 0$ now takes the form of an incomplete version of the beta function from equation (21), corresponding to an integral[12] evaluated from c to $2c$ rather than extending to infinity. This inner product does not however correspond to a mode expansion of the field, since the analytic continuation of the diamond would be to all of W_c, or all of $\widetilde{W_{2c}}$, in which case the mode would no longer be localized to the diamond. So it is no longer invariant to integrate along a Cauchy surface for the inner product; this construction does not define a complete orthonormal set, and cannot be used to build a full basis of field modes.

This motivates a shift in perspective: rather than interpreting r_q as part of a global mode expansion, we regard it as a compactly supported, non-invariant test function, i.e., a driving source localized to the diamond region, consistent with the source framework introduced in Section 3. We turn on r_q exactly for a fixed period of $x - t$ (or $x + t$ for r_{-q}).

[12]We could also use the other form of the beta function in equation (22) to compute the same inner product.

The resulting spectral response in the diamond, computed from this truncated integral, is shown[13] in Figure 9.

The plot reveals that the main spectral peak at $\omega_k = \omega_q$ persists, while the thermal contribution near $\omega = 0$ is significantly attenuated.

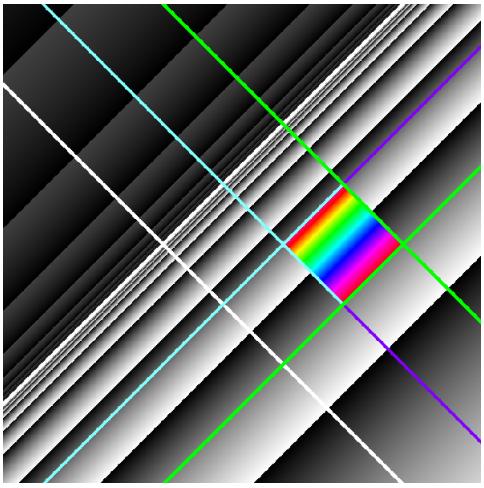

Figure 10: The same situation as in Figure 8 but we further intersect with a reflected (left) wedge $\widetilde{W}_{2c}$ (green). Rindler mode r_q of W_0 (gray-scale) restricted to $W_c \cap \widetilde{W}_{2c}$ (rainbow).

4.3 Thermal to Localized Interpolation

To further probe how global thermal structure transitions into a localized excitation, we consider the behavior of Rindler-to-Minkowski Bogoliubov coefficients when weighted by a Gaussian envelope. This allows us to interpolate between de-localized (thermal) and localized (spectrally peaked) behavior. We use parabolic cylinder functions [11, 12] which are the analytic continuation of

$$D_\nu(-z) = \frac{e^{-\frac{1}{4}z^2}}{\Gamma(-\nu)} \int_0^\infty \mathrm{d}s \; e^{zs} s^{-\nu-1} e^{-\frac{1}{2}s^2}, \Re\nu < 0, \tag{38}$$

where we use $-z$ instead of the usual z so that future equations become simpler.

Without loss of generality, let $N_{\mu,\sigma} = e^{-\frac{1}{2}\frac{(x-t-\mu)^2}{\sigma^2}}$ be a (left-moving) Gaussian kernel with fixed μ. We will multiply φ_q^* by $N_{\mu,\sigma}$, but we could just as easily multiply r_k by $N_{\mu,\sigma}$ for the same effect. A key aspect of this construction is that the resulting Minkowski modes are treated as driving sources rather than elements of an orthonormal mode expansion. Since we are not working within an orthonormal mode expansion, the normalization of $N_{\mu,\sigma}$ is left implicit. For clarity, since this setup may be non-standard, we carry out the calculations explicitly in this section. We will examine the $N_{\mu,\sigma}$ modification of $\beta_{kq}^{(c\to M)}$ in equation (20)

[13]The green (complete) beta function curve is actually independent of the choice of translation c, it is the same curve for any sub-wedge space-like inclusion (see modular automorphism Section 2.4). In contrast, the incomplete beta function curve (magenta) does depend on the endpoint ($2c$ is shown).

$$
\begin{aligned}
\left\langle \varphi_q^* N_{\mu,\sigma}, r_k \right\rangle &= \frac{1}{4\pi\sqrt{\omega_q \omega_k}} 2i \int_{\Sigma_W} e^{-i(\omega_q t - qx)} e^{-\frac{1}{2}\frac{(x-t-\mu)^2}{\sigma^2}} \partial_t (a(x-t))^{\frac{i\omega_k}{a}} \\
&= \frac{1}{2\pi}\sqrt{\frac{\omega_k}{\omega_q}} a^{\frac{i\omega_k}{a}-1} \int_0^\infty \mathrm{d}x \; e^{-\frac{1}{2}\frac{(x-\mu)^2}{\sigma^2}+iqx} x^{\frac{i\omega_k}{a}-1} \\
&= \frac{1}{2\pi}\sqrt{\frac{\omega_k}{\omega_q}} a^{\frac{i\omega_k}{a}-1} \int_0^\infty \mathrm{d}x \; e^{\left(-\frac{1}{2\sigma^2}\right)x^2+\left(\frac{\mu}{\sigma^2}+iq\right)x+\left(-\frac{\mu^2}{2\sigma^2}\right)} x^{\frac{i\omega_k}{a}-1} \\
&= \frac{1}{2\pi a}\sqrt{\frac{\omega_k}{\omega_q}} e^{-\frac{\mu^2}{2\sigma^2}} \sigma^{\frac{i\omega_k}{a}} a^{\frac{i\omega_k}{a}} \int_0^\infty \mathrm{d}s \; e^{(\frac{\mu}{\sigma}+iq\sigma)s} s^{\frac{i\omega_k}{a}-1} e^{-\frac{1}{2}s^2} \\
&= \frac{1}{2\pi a}\sqrt{\frac{\omega_k}{\omega_q}} e^{-\frac{\mu^2}{2\sigma^2}} (\sigma a)^{\frac{i\omega_k}{a}} e^{\frac{1}{4}(iq\sigma+\frac{\mu}{\sigma})^2} \Gamma\left(\frac{i\omega_k}{a}\right) D_{-\frac{i\omega_k}{a}}(-iq\sigma - \frac{\mu}{\sigma}) \\
&= \frac{1}{2\pi a}\sqrt{\frac{\omega_k}{\omega_q}} e^{-\frac{\mu^2}{2\sigma^2}} (\sigma a)^{\frac{i\omega_k}{a}} e^{\frac{1}{4}z^2} \Gamma(-\nu) D_\nu(-z)
\end{aligned}
\tag{39}
$$

where Σ_W is the Cauchy surface $\eta = 0$ on the Rindler wedge W, $x = \sigma s$, $z = iq\sigma + \frac{\mu}{\sigma}$, and $\nu = -\frac{i\omega_k}{a}$. And then

$$
\left|\left\langle \varphi_q^* N_{\mu,\sigma}, r_k \right\rangle\right|^2 = \frac{1}{2\pi a \omega_q} \frac{\omega_k}{2\pi a} e^{-\frac{\mu^2}{\sigma^2}} \left| e^{\frac{1}{2}z^2} \right| |\Gamma(-\nu)|^2 \, |D_\nu(-z)|^2 \tag{40}
$$

From [12] we have

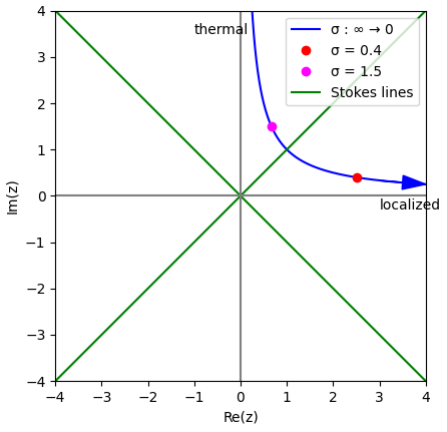

Figure 11: Trajectory of $z = iq\sigma + \frac{\mu}{\sigma}$ as σ interpolates between thermal and localized regimes. For σ starting at ∞, the trajectory starts at the positive infinite imaginary axis, aligning with the dominant thermal component of the excitation. As $\sigma \to 0$, the system crosses a Stokes line and transitions into a sharply localized, source-driven configuration, where thermal character disappears. See also corresponding Figure 12.

$$
D_\nu(-z) = e^{-i\pi\nu} z^\nu e^{-\frac{1}{4}z^2} \{1 + O(|z|^{-2})\} + \frac{(2\pi)^{\frac{1}{2}}}{\Gamma(-\nu)} z^{-\nu-1} e^{\frac{1}{4}z^2} \{1 + O(|z|^{-2})\} \tag{41}
$$

when $-\frac{1}{4}\pi + \epsilon \leq \arg z \leq \frac{3}{4}\pi - \epsilon$.

The two asymptotic regimes correspond to physically distinct interpretations: The second $e^{\frac{1}{4}z^2}$ term dominates for $z \to \infty$ as $\sigma \to 0$ and the first $e^{-\frac{1}{4}z^2}$ term dominates for

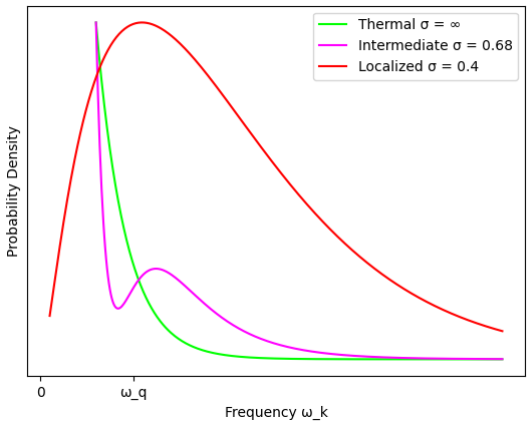

Figure 12: $\left|\left\langle \varphi_q^* N, r_k \right\rangle\right|^2$ for various values of σ (probability density is scaled for comparison). $\omega_q = 1$, $q = 1$, $a = 1$, $\mu = 1$. See also corresponding Figure 11.

$z \to i\infty$ as $\sigma \to \infty$. This is a Stokes phenomenon[14] which flips over as we cross the Stokes line at $\arg z = \frac{\pi}{4}$. The situation is pictured in Figure 11.

We next combine equations (40) and (41). First for the thermal part that comes from the $e^{-\frac{1}{4}z^2}$ term where $\sigma \to \infty$ we have

$$\begin{aligned} 2\pi a\omega_q \left|\left\langle \varphi_q^* N, r_k \right\rangle\right|^2 &= \frac{\omega_k}{2\pi a} e^{-\frac{\mu^2}{\sigma^2}} \left| e^{-i\pi\nu} z^\nu \Gamma\left(\frac{i\omega_k}{a}\right)\right|^2 \\ &= \frac{\omega_k}{2\pi a} e^{-\frac{\mu^2}{\sigma^2}} e^{\frac{-2\pi\omega_k}{a}} \left| e^{\frac{-2i\omega_k}{a}\log\left(\frac{\mu}{\sigma}+iq\sigma\right)}\right|^2 \frac{\pi}{\frac{\omega_k}{a}\sinh\frac{\pi\omega_k}{a}} \\ &\to e^{\frac{-2\pi\omega_k}{a}} \left| e^{\frac{-2i\omega_k}{a}\log i}\right|^2 \frac{1}{2\sinh\frac{\pi\omega_k}{a}} \\ &= e^{\frac{-2\pi\omega_k}{a}} e^{\frac{\pi\omega_k}{a}} \frac{1}{\left(e^{\frac{\pi\omega_k}{a}} - e^{\frac{-\pi\omega_k}{a}}\right)} \\ &= \frac{1}{e^{\frac{2\pi\omega_k}{a}} - 1} \end{aligned} \tag{42}$$

which we expect by construction. For the localized part that comes from the $e^{\frac{1}{4}z^2}$ term where $\sigma \to 0$ we have

$$\begin{aligned} 2\pi a\omega_q \left|\left\langle \varphi_q^* N, r_k \right\rangle\right|^2 &= \frac{\omega_k}{a} e^{-\frac{\mu^2}{\sigma^2}} \left| e^{z^2} z^{2(-\nu-1)}\right| \\ &= \frac{\omega_k}{a} e^{-\frac{\mu^2}{\sigma^2}} \left| e^{\left(iq\sigma+\frac{\mu}{\sigma}\right)^2} e^{2\left(\frac{i\omega_k}{a}-1\right)\log\left(iq\sigma+\frac{\mu}{\sigma}\right)}\right| \\ &\to \frac{\omega_k}{a} e^{\frac{-2\epsilon\omega_k}{a}} f(\sigma,\mu) \end{aligned} \tag{43}$$

where the thermal pole at zero has disappeared. While the precise asymptotic form is not critical, we can control the ultraviolet behavior by taking z to $(1+i\epsilon)\infty$ which remains within in the localized Stokes region. This introduces a regulating factor of the form $e^{-2\epsilon\omega_k/a}$, which suppresses high-frequency contributions.

We should stop short of σ actually reaching zero, since that is a localization to an extreme, where $N_{\mu,\sigma}$ shrinks to a bump with infinitesimal width; this is not a delta function, it is a vanishing source. We focus on the small-but-nonzero σ regime where the

[14] See [13] for a similar approach where the Stokes phenomenon is applied to particle production in simple expanding backgrounds, preheating after R^2 inflation, and a transition model with smoothly changing mass.

thermal character has already disappeared. See Figure 12 for representative plots across varying values of σ.

5 Future Research

Several directions naturally extend the present work:

- **Moving Mirrors**. While a moving mirror can be interpreted as a type of thruster that reshapes the field through boundary acceleration, here we isolated the thruster from the detector role. Incorporating moving mirror timeline localizations into this framework remains an open task.
- **Mode Pairing**. The construction of f_L in Section 3 was left aside in our treatments in Section 4. A more systematic analysis of the pairing between f_L and f_R would allow us to track correlations in greater generality.
- **Alternative Driving Sources**. Beyond entangled emission, one may consider models involving single-photon sources or even time-reversed scenarios (see Section 3.2), which could offer finer control over the entanglement structure.
- **Massive Fields**. Extending the analysis to massive scalar fields would open the possibility of studying localized virtual particle–antiparticle pair production, complementing the massless case.
- **Curved Spacetimes**. While our analysis is grounded in flat spacetime, the equivalence principle offers a natural pathway to curved geometries. In particular, applications to Hawking radiation could be explored by modeling localized excitations near black hole horizons. Figure 13 illustrates this direction, highlighting a shift from thermal emission to localized, physically sourced excitations in the near-horizon region.

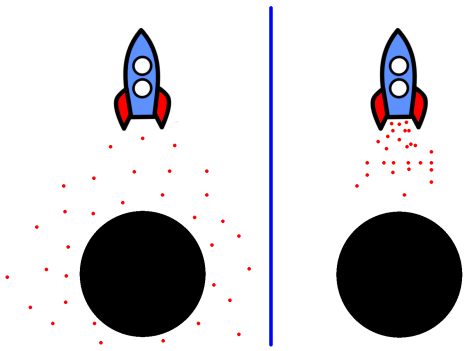

Figure 13: Conceptual illustration contrasting global Hawking radiation (left) with a localized, source-driven excitation near a black hole (right). Compare with Figure 5.

6 Conclusion

This work examined the Unruh phenomenon from a localized perspective, emphasizing its manifestation as a physically driven effect rather than a purely thermal one. By restricting Rindler modes to translated and reflected wedges, and their intersections, we showed that the apparent thermal behavior can be partially eliminated. As these modes become localized, the traditional detector response, typically interpreted as a thermal signature of entanglement across a causal horizon, is here reinterpreted as the spectral imprint of

a localized, dynamically sourced excitation. We then showed that the mixed Bogoliubov inner product between Minkowski and Rindler modes provides a smooth interpolation from global thermality to a localized spectral structure, with parabolic cylinder functions encoding this transition in analytic form.

Our approach complements the traditional detector-based interpretation by highlighting the role of the physical agent behind acceleration as an active source of field excitations. This perspective does not contradict the well-known thermality arising from entanglement but offers a localized, dynamical viewpoint that may better capture future experimental scenarios. In this picture, the Unruh response may be linked in part to "thrust particles", in the sense of Section 3, potentially contributing to an attenuation of the isotropic random signal.

7 Acknowledgments

I thank Frodden and Valdés for their excellent exposition [2], and Beisert for his insightful lecture notes [14]. I'm also grateful to Ben Commeau, Daniel Justice, Edward Randtke, and ChatGPT for helpful discussions.

References

[1] W. G. Unruh, "Notes on black-hole evaporation," *Physical Review D*, vol. 14, no. 4, p. 870, 1976.

[2] E. Frodden and N. Valdes, "Unruh effect: Introductory notes to quantum effects for accelerated observers," *International Journal of Modern Physics A*, vol. 33, no. 27, p. 1830026, 2018.

[3] W. Rindler, "Kruskal space and the uniformly accelerated frame," *Am. J. Phys*, vol. 34, no. 12, pp. 1174–1178, 1966.

[4] R. Bracewell and P. B. Kahn, "The fourier transform and its applications," *American Journal of Physics*, vol. 34, no. 8, pp. 712–712, 1966.

[5] H. J. Borchers, "On revolutionizing quantum field theory with tomita's modular theory," *Journal of mathematical Physics*, vol. 41, no. 6, pp. 3604–3673, 2000.

[6] A. Einstein, *General Relativity: An Einstein Centenary Survey*. Cambridge University Press, 1979.

[7] S. A. Fulling and P. C. Davies, "Radiation from a moving mirror in two dimensional space-time: conformal anomaly," *Proceedings of the Royal Society of London. A. Mathematical and Physical Sciences*, vol. 348, no. 1654, pp. 393–414, 1976.

[8] J. Schwinger, "Particles and sources," *Physical Review*, vol. 152, p. 1219â€"1226, Dec. 1966.

[9] L. H. Ryder, *Quantum field theory*. Cambridge university press, 1996.

[10] C. C. Gerry and P. L. Knight, *Introductory quantum optics*. Cambridge university press, 2023.

[11] M. Abramowitz and I. A. Stegun, eds., *Handbook of Mathematical Functions with Formulas, Graphs, and Mathematical Tables*, vol. 55 of *Applied Mathematics Series*. Washington, D.C.: U.S. Government Printing Office, 1964. Reprinted 1983. See Chapter 19.

[12] F. W. J. Olver, "Uniform asymptotic expansions for weber parabolic cylinder functions of large orders," *Journal of Research of the National Bureau of Standards. Section B, Mathematical Sciences*, vol. 63B, pp. 131–169, 1959.

[13] S. Hashiba and Y. Yamada, "Stokes phenomenon and gravitational particle production—how to evaluate it in practice," *Journal of Cosmology and Astroparticle Physics*, vol. 2021, no. 05, p. 022, 2021.

[14] N. Beisert, "Quantum field theory i," *ETH Zurich, HS12*, 2012.